CHEMISTRY OF MATERIALS

pubs.acs.org/cm

Article

Colossal Chromatic Shift in the $Ba_2Ca_2B_4O_{10}:Ce^{3+}$ Phosphor

Małgorzata Sójka, Shruti Hariyani, Nakyung Lee, and Jakoah Brgoch*

Cite This: *Chem. Mater.* 2023, 35, 6491−6501

Read Online

ACCESS | Metrics & More | Article Recommendations | Supporting Information

ABSTRACT: Developing high-color-quality white light-emitting diodes (LEDs) is crucial for energy-efficient light bulbs and modern flat panel displays. Creating the luminescent phosphors that enable these advanced lighting technologies requires stable photoluminescence under varying temperatures. In this study, we examine $Ba_2Ca_2B_4O_{10}$ substituted with Ce^{3+}, which emits an efficient blue-cyan light ($\lambda_{em} \approx 455$ nm and a quantum yield of 74%) that is required for high color rendering lighting. Synchrotron powder X-ray diffraction and optical spectroscopy reveal that the broad emission band is attributed to Ce^{3+} ions occupying two crystallographically independent Ba^{2+} positions in the host crystal structure. However, temperature-dependent luminescence measurements unveil a surprising phenomenon: a significant blue shift (from 460 to 415 nm) accompanied by a drastic narrowing of the total emission bandwidth (from 140 nm, 6900 cm^{-1} to 58 nm, and 3200 cm^{-1}). This extreme optical response arises from two simultaneous thermal quenching mechanisms—site preferential quenching and high thermal expansion ($\alpha_V \approx 5.39 \times 10^{-5}$ K^{-1}). Consequently, the phosphor experiences a chromatic shift that transforms a fabricated prototype light bulb's perceived color from functional white light to an undesirable yellow-green hue. These findings underscore the considerable impact of chromatic instabilities in phosphors and the effects they can have on the performance of LED lighting.

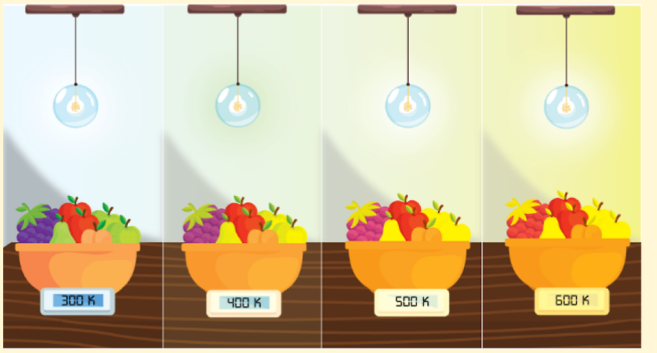

1. INTRODUCTION

Solid-state lighting is quickly replacing incandescent and compact fluorescent light bulbs due to their lower energy use, higher illuminance, longer operational lifetimes, and mercury-free components.[1,2] The ongoing, government-driven push to phase out fluorescent lights in favor of a more energy-efficient technology will surely drive the adoption rates of phosphor-converted light-emitting diodes (pc-LED) higher. Thus, it is unsurprising that the pc-LED market is expected to reach $133 billion by 2030, with an annual growth rate of 10.5%.[3]

The most common solid-state light bulbs sold today operate by combining a blue-emitting InGaN LED chip ($\lambda_{em} \approx 450$ nm) with multiple inorganic phosphors such as yellow-emitting $(Y_{3-x}Ce_x)Al_5O_{12}$ (YAG:Ce) and red-emitting $(Sr_{2-x}Eu_x)$-Si_5N_8.[4,5] Phosphors are composed of rare-earth ions that are substituted within a host crystal structure, which partially absorb the blue emission produced by the LED chip and down-convert these photons to lower energy (longer wavelengths). The combination of the blue, yellow, and red emissions appears as white light to the average human eye. Regrettably, the lack of photons in the 400−450 nm spectral range and the 480−520 nm spectral range, termed the cyan gap, among other spectral coverage issues, limit the white light's overall capability for color rendering, resulting in a lower than desired color rendering index (CRI) R_a of ≈80.[2] As a result, one proposed alternative to improve the color rendering of pc-LEDs is to utilize a violet ($\lambda_{em} = 395$ nm) or ultraviolet (UV, $\lambda_{em} = 365$ nm) LED chip coated with a trichromatic (a broad blue-cyan, green-, and red-emitting) phosphor mixture.[1,6] Undoubtedly, the inclusion of three distinct phosphors can lead to improved coverage of the visible spectrum, yielding a remarkable improvement in the CRI R_a score to >90.[1]

However, several limiting factors prevent the practical application of these violet ($\lambda_{em} \approx 395$ nm) or UV ($\lambda_{em} \approx 365$ nm)-based device architectures today. The most notable is the high cost of GaN LED chips. Synthesis of GaN uses an expensive silicon carbide substrate to reduce lattice mismatch. Traditional InGaN LEDs ($\lambda_{em} \approx 450$ nm), on the other hand, can be grown on cheaper Si substrates with a minimal lattice mismatch.[7] There are also challenges associated with the trichromatic phosphor blend. All the three phosphors must demonstrate a photoluminescence quantum yield (PLQY) near unity to counteract the inherent Stokes losses from the phosphor down-conversion process. There has been some

Received: June 12, 2023
Revised: July 17, 2023
Published: August 2, 2023

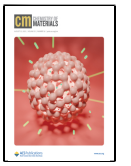

progress in identifying new systems with an exceptionally high PLQY, although this is still not trivial.[8] The three phosphors must also age similarly over the device's lifecycle. As a result, significant effort has gone into optimizing and commercializing numerous UV or violet excitable phosphors like green emitting β-SiAlON:Eu^{2+}, $Ca_3Sc_2Si_3O_{12}$:Ce^{3+}, $SrSi_2O_2N_2$:Eu^{2+}, γ-MgAlON:Mn^{2+},[9−12] and red emitters like Ca_2SiO_4:Eu^{2+}, Sr[$LiAl_3N_4$]:Eu^{2+}, $Sr_2Si_5N_8$:Eu^{2+}, and $CaAlSiN_3$:Eu^{2+}.[13−16] Unfortunately, there is only one viable blue-emitting phosphor that can be used in these pc-LEDs. $BaMgAl_{10}O_{17}$:Eu^{2+} (BAM:Eu^{2+})[17] can be excited by UV or violet radiation, producing bright blue luminescence with a remarkable PLQY of ≈99% (λ_{ex} = 365 nm) stemming from years of rigorous post-processing. However, BAM:Eu^{2+} still experiences a decrease in luminescence intensity over prolonged usage due to oxidation of the luminescent center from Eu^{2+} to Eu^{3+}.[18] The material is also sensitive to long-term water exposure, resulting in a red shift accompanied by a broadening of the emission spectrum.[19]

Additional issues arise in devices containing a trichromatic phosphor blend when considering the operating temperatures of modern high-power pc-LED lights. Temperature-driven fluctuations can cause significant changes in the vibrational molecular dynamics and electron−phonon interactions within the rare-earth−host structure combination, leading to perturbations in the emission intensity, full width at half-maximum (fwhm), and peak position ($\lambda_{em,max}$) of each phosphor.[20,21] Bearing in mind that pc-LEDs can reach temperatures up to 423 K (150 °C) during operation, the phosphors' spectroscopic features must be retained at elevated temperatures.[1] Therefore, phosphors are only considered thermally robust if they undergo minimum thermal quenching and have a T_{50}, which is defined as the temperature where the luminescence intensity is 50% of the room temperature value, above 423 K. Changes in the phosphor's intensity, fwhm, and $\lambda_{em,max}$ can also substantially affect the observed color of the emitted light. The concept of color differences in white lighting is commonly expressed through a MacAdam ellipses analysis. According to industry guidelines, the emission color of a phosphor should stay within a three-step MacAdam ellipse, indicating that any color change is not discernible to the human eye.[22] Presently, the techniques for obtaining phosphors with a thermally stable color point are uncertain, which highlights the need to establish correlations between the phosphor's crystal chemistry and chromatic stability.

Borates have recently regained considerable attention as promising host structures for Ce^{3+} substitution. This is due to the moderate centroid shift, which can facilitate the occurrence of 5d → 4f rare-earth electronic transitions generally within the blue-cyan region of the electromagnetic spectrum, which is needed for applications in UV or violet LED-based devices. More importantly, borate phosphors tend to exhibit excellent thermal and chromatic stability, maintaining intense photoluminescence even at high temperatures (T > 450 K). They also tend to have accessible synthetic routes, and their diverse crystal chemistries enable tunable optical properties from the UV to the blue part of the electromagnetic spectrum. Some notable borate phosphors with great thermal stability that have recently been published include $NaMgBO_3$:Ce^{3+} (T_{50} > 500 K), $KCa_4(BO_3)_3$:Ce^{3+} (T_{50} > 523 K), and $Ba_3Y_2B_6O_{15}$:Ce^{3+} (T_{50} > 394 K).[23−25] One underexplored compositional space is the BaO−CaO−B_2O_3 system. Only three compounds have been reported in this composition space: $Ba_2CaB_6O_{12}$,[26] $Ba_2CaB_2O_6$,[27] and $Ba_2Ca_2B_4O_{10}$.[28] The first two materials show efficient blue luminescence upon substitution with Ce^{3+} or Eu^{2+}.[29−31] There is no convincing explanation in the literature about which site the luminescence ion will occupy in these materials, limiting our ability to interpret their optical properties. However, temperature-dependent luminescence measurements of $Ba_2CaB_2O_6$:Ce^{3+} reveal its high thermal stability with a T_{50} = 640 K.[30] Surprisingly, $Ba_2Ca_2B_4O_{10}$, which crystallizes in the $P2_1/c$ space group, has never been investigated as a phosphor. Given the desirable properties of the analogous systems in this composition space, this borate will likely yield excellent optical properties.

In this work, we investigate the connection between the chemical composition, crystal, structure, and optical response of $Ba_2Ca_2B_4O_{10}$:Ce^{3+}. The target product was prepared via solid-state synthesis and characterized using synchrotron X-ray diffraction and Rietveld refinements, which indicate that Ce^{3+} exclusively occupies the Ba^{2+} sites. Detailed luminescence measurements reveal efficient blue-cyan photoluminescence under 360 nm excitation (PLQY = 74(1)%), making it viable for UV LED device incorporation. However, temperature-dependent luminescence measurements show an intriguing optical response. Thermal quenching occurs at 340 K, while a more intriguing dramatic emission blue-shift from 470 to 415 nm (≈21,000−24,000 cm^{-1}) occurs as the temperature increases from 300 to 640 K. This shift is attributed to two mechanisms. First, temperature-induced site-selective quenching narrows the fwhm from ≈140 to 58 nm (≈6900−3300 cm^{-1}). Temperature-dependent powder X-ray diffraction shows that this phosphor also has a large thermal expansion coefficient, which influences the local structure and further induces a blue shift in the photoluminescence. In combination, a colossal chromatic shift is observed in $Ba_2Ca_2B_4O_{10}$:Ce^{3+}. Finally, constructing a prototype device demonstrates the impact a phosphor with poor thermal response can have on a device's overall optical response. Understanding the properties of this phosphor provides an insight into the design of other phosphors with better chromatic stability required for next-generation LED lighting.

2. EXPERIMENTAL SECTION

2.1. Synthesis. Polycrystalline samples of $Ba_{2-(3/2)x}Ce_xCa_2B_4O_{10}$ (x = 0.005, 0.01, 0.02, 0.03, and 0.05) were prepared via high-temperature solid-state synthesis starting from $BaCO_3$ (Johnson Matthey, 98%), $CaCO_3$ (Alfa Aesar, 99%), H_3BO_3 (Sigma-Aldrich, 99.999%), and CeO_2 (Sigma-Aldrich, 99.995%). The starting materials were weighed according to the required stoichiometric ratio, with a 3% excess of $CaCO_3$ to compensate for potential evaporation during synthesis, and thoroughly ground in an agate mortar using acetone as a grinding medium. The powders were subsequently milled in a high-energy ball mill (Spex 8000 M Mixer/Mill) for 30 min. The as-prepared mixture was then heated in a box furnace in the air at 700 °C for 5 h to decompose the starting reagents. The samples were reground and heated at 850 °C for 10 h in a silica tube furnace under a reducing atmosphere (5% H_2/95% N_2) with heating and cooling rates of 3 °C min^{-1}. The $Ba_2Y_5B_5O_{17}$:2% Ce^{3+} and $Ba_3Y_2B_6O_{15}$:2% Ce^{3+} phosphors were synthesized according to the previously published work.[25,32]

2.2. Characterization. Powder X-ray diffraction confirmed the phase purity of all investigated compositions (Panalytical X'Pert Pro; Cu Kα radiation λ = 1.5406 Å). Temperature-dependent powder X-ray diffractograms were collected using an Anton-Paar TTK450 chamber and measured on an X'Pert3 PANalytical with Cu Kα radiation. Le Bail refinements were performed on all diffractograms using the EXPGUI interface and General Structure Analysis System (GSAS) software with a shifted Chebyshev function employed to fit

https://doi.org/10.1021/acs.chemmater.3c01465
Chem. Mater. 2023, 35, 6491−6501

the background.[33] Rietveld refinements of the $Ba_2Ca_2B_4O_{10}$ host structure and $Ba_{2-(3/2)x}Ce_xCa_2B_4O_{10}$ were performed on synchrotron X-ray powder diffraction collected at 298 K on beamline 11-BM at the Advanced Photon Source (λ = 0.412835 Å). The refined crystal structures were visualized using VESTA.[34]

Luminescence measurements were performed by encapsulating the investigated materials in silicone resin (United Adhesives Inc., OP 4036) and depositing the mixture in a quartz slide (Chemglass). Photoluminescent spectra were recorded on a PTI fluorescence spectrophotometer using a 75 W xenon arc lamp as a continuous excitation light source. Excitation and emission spectra were corrected for the incident light intensity and the wavelength dependence of the spectral response of the recording system, respectively. The room-temperature PLQY was determined following the method of de Mello et al.[35] where the sample slides are placed in a Spectralon-coated integrated sphere (150 mm diameter, Labsphere) and excited using 355 nm. Temperature-dependent emission and excitation spectra were collected using a Janis liquid nitrogen cryostat (VPF-100) in the 80 to 640 K range.

Fabrication of a pc-LED involved using $Ba_{1.97}Ce_{0.02}Ca_2B_4O_{10}$ with commercially available β-SiAlON:Eu^{2+} (Mitsubishi Chemical Corporation) and $Sr_2Si_5N_8$:Eu^{2+} (Stanford Advanced Materials). The ratio of each phosphor was optimized to 5.81 wt % $Sr_2Si_5N_8$:Eu^{2+}, 56.42 wt % $Ba_{1.97}Ce_{0.02}Ca_2B_4O_{10}$, and 2.57 wt % of β-SiAlON:Eu^{2+} for the 365 nm LED device.

2.3. Computation. The Vienna Ab Initio Simulation Package (VASP) was utilized for density functional theory (DFT) calculations.[36] All calculations employed a plane-wave basis set with projector-augmented wave (PAW) pseudopotentials.[37] The host crystal structure was relaxed using the generalized gradient approximation (GGA) Perdew–Burke–Ernzerhof (PBE) functional.[38] The Debye temperature, $\Theta_{D,DFT}$, was determined using the quasi-harmonic Debye model. Here, $\Theta_{D,DFT}$ is approximated based on the spherical average of the sound velocity and is determined following eq 1, where k_B and $\hbar$ are the Boltzmann and Planck's constants, respectively, V is the optimized volume of the unit cell, and n_a is the number of atoms in the unit cell. The elastic moduli, including the bulk modulus, B_H, and ν, the Poisson ratio, were determined using the Voigt–Reuss–Hill (VRH) approximation based on the elastic constants, C_{ij}, following the method of Wu et al.[39] The value of $f(\nu)$ is determined using eq 2.

$$\Theta_D = \frac{\hbar}{k_B}[6\pi^2 V^{1/2} n_a]^{1/3}\sqrt{\frac{B_H}{M}}f(\nu) \quad (1)$$

$$f(\nu) = \left\{3\left[2\left(\frac{2}{3}\frac{1+\nu}{1-2\nu}\right)^{3/2} + \left(\frac{1}{3}\frac{1+\nu}{1-2\nu}\right)^{3/2}\right]^{-1}\right\}^{1/3} \quad (2)$$

In addition to the elastic constants, the density of states and bandgap were also calculated. The exchange and correlation were described using the Heyd–Scuseria–Ernzerhof screened hybrid functional, HSE06, which implements a 75:25 mixture of the PBE/Hartree–Fock functionals with a range separation of 0.2 Å to account for the significant underestimation of the bandgap when using the PBE functional alone.[40] Post-processing was conducted using the VASPKIT package.[41] The electronic structure and ionic force convergence criteria were set to 1×10^{-6} eV and 1×10^{-6} eV/Å, respectively. A cutoff energy of 500 eV was used for the basis set of the plane waves, and a $6 \times 2 \times 4$ Γ-centered Monkhorst–Pack k-point grid was used to sample the first Brillouin zone.

3. RESULTS AND DISCUSSION

3.1. Synthesis, Structure, and Photoluminescence. There has been a revival in the search for borate phosphors due to their wide electronic bandgaps (E_g) and boron's small size, which allows for dense polyhedral packing and gives rise to high Debye temperatures (Θ_D).[8] This combination generally reduces access to non-radiative quenching pathways yielding highly efficient and thermally stable phosphors. For instance, $Na(Ba_{1-x}Eu_x)B_9O_{15}$ exhibits a remarkably high PLQY (≈95%, λ_{ex} = 320 nm) and zero thermal quenching that can be attributed to a rigid structural backbone signified by the high DFT-calculated Debye temperature, $\Theta_{D,DFT}$, of 635 K and a wide E_g of 7.3 eV.[42] Similarly, the wide E_g (≈5.5 eV) of $(Na_{1-x}Ce_x)MgBO_3$ was shown to prevent photoionization, while the high Θ_D (≈563 K) prevented other non-radiative pathways, resulting in a high PLQY of 93%.[23] The electronic band structure of $Ba_2Ca_2B_4O_{10}$ depicted in Figure 1a was

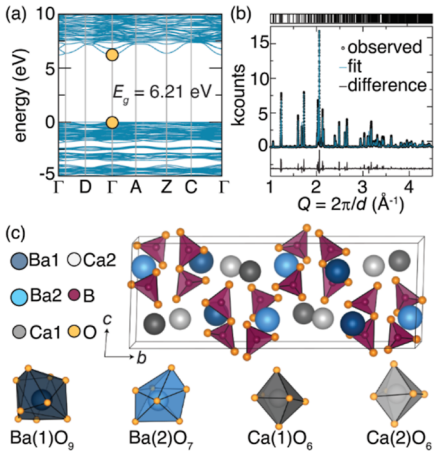

Figure 1. (a) The band structure of $Ba_2Ca_2B_4O_{10}$ was calculated through the HSE06 hybrid functional showing a direct bandgap (E_g) of 6.21 eV. (b) Rietveld refinement of synchrotron powder X-ray diffractogram for $(Ba_{1.97}Ce_{0.02})Ca_2B_4O_{10}$. (c) Crystal structure of the $Ba_2Ca_2B_4O_{10}$ host with possible substitution polyhedral units [Ba(1)O_9], [Ba(2)O_7], [Ca(1)O_6], and [Ca(2)O_6] highlighted.

therefore calculated using the HSE06 hybrid functional and revealed a direct bandgap of 6.21 eV. The calculated $\Theta_{D,DFT}$ was determined to be 532 K, indicating high structural rigidity.[8] These results suggest that $Ba_2Ca_2B_4O_{10}$ should similarly produce highly efficient and thermally robust photoluminescence.

$Ba_2Ca_2B_4O_{10}$, as a pristine, an unsubstituted crystal structure, has been previously synthesized at 900 °C for 72 h with several intermittent grindings.[28] However, implementing this synthetic methodology resulted in a final product with poor crystallinity, accompanied by notable impurities from ternary borates. The desired phase was eventually obtained through a two-step synthesis involving mixing Ba_2CO_3, $CaCO_3$, H_3BO_3, and CeO_2 and sintering at 700 °C for 5 h in air. The mixture was reground and heated at 850 °C for 10 h in a reducing atmosphere of H_2/N_2. The body color of the final powder was white. The laboratory powder X-ray diffractograms confirm the near-phase purity of the loaded compositions $Ba_{2-(3/2)x}Ce_xCa_2B_4O_{10}$ (x = 0.005, 0.01, 0.02, 0.03, and 0.05). The addition of the rare-earth ion gradually shifted the host structure's diffraction peaks toward higher angles, as illustrated in Figure S1a. Le Bail refinements confirm that the refined unit cell volume shrinks almost linearly from 981.5(2) to 978.5(4) Å as a function of increasing Ce^{3+} concentration (Figure S1b). This change follows Zen's law[43] and is consistent with the smaller Ce^{3+} ($r_{7\text{-coord}}$ = 1.07 Å and $r_{9\text{-coord}}$ = 1.196 Å) substituting upon Ba^{2+} ($r_{7\text{-coord}}$ = 1.38 Å and $r_{9\text{-coord}}$ = 1.47 Å) over the Ca^{2+} ($r_{7\text{-coord}}$ = 1.06 Å, $r_{9\text{-coord}}$ = 1.18 Å) positions.[44]

https://doi.org/10.1021/acs.chemmater.3c01465
Chem. Mater. 2023, 35, 6491–6501

The compositions were further characterized by high-resolution synchrotron powder X-ray diffraction to obtain more accurate structural information. Rietveld refinements of $(Ba_{1.97}Ce_{0.02})Ca_2B_4O_{10}$ and the pristine $Ba_2Ca_2B_4O_{10}$ host are provided in Figures 1b and S2, respectively. The results of the refinements are provided in Table 1, and the refined atomic coordinates are shown in Tables S1 and S2. $Ba_2Ca_2B_4O_{10}$ crystallizes in the monoclinic space group $P2_1/c$ (no. 14). The structure contains four crystallographically independent positions that Ce^{3+} could occupy: two Ba^{2+} sites and two Ca^{2+} sites, as illustrated in Figure 1c. The Ba^{2+} ions are coordinated by seven or nine oxygen atoms forming distortional face-capped octahedra and tricapped octahedra, respectively. The Ca^{2+} ions are connected to six oxygen atoms forming a pair of distorted octahedra. The polyhedral units are subsequently interlinked by distorted trigonal $[BO_3]$ prisms and isolated $[B_2O_5]$ units, as depicted in Figure 1c. The results of the Rietveld refinement are consistent with the initial Le Bail refinement, where the refined unit cell volume decrease with the presence of Ce^{3+}, suggesting the incorporation of the rare-earth ions primarily on the two crystallographically independent Ba^{2+} positions. Unfortunately, direct refinement of Ce^{3+} occupancy in the crystal structure is not possible even with synchrotron scattering, given its low concentration and a similar scattering factor to Ba^{2+}.

Table 1. Rietveld Refinement Data of $Ba_2Ca_2B_4O_{10}$ and $Ba_{1.97}Ce_{0.02}Ca_2B_4O_{10}$

nominal composition	$Ba_2Ca_2B_4O_{10}$	$(Ba_{1.97}Ce_{0.02})Ca_2B_4O_{10}$
radiation type; λ (Å)	synchrotron; 0.457667	synchrotron; 0.457667
Q range (Å^{-1})	0.8−8.00	0.8−8.00
temperature (K)	298 K	298 K
space group; Z	$P2_1/c$	$P2_1/c$
a (Å)	6.5739(1)	6.5703(1)
b (Å)	20.5526(1)	20.5333(1)
c (Å)	8.1981(1)	8.1805(1)
β (deg)	117.0211(2)	116.99(1)
unit cell volume (Å^3)	986.75(1)	983.47(1)
R_p	0.1126	0.0976
R_{wp}	0.1398	0.1257
χ^2	4.212	3.982

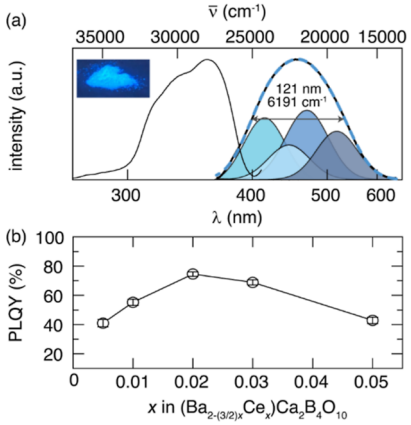

Figure 2. (a) Excitation (λ_{em} = 460 nm) and emission (λ_{ex} = 355 nm) spectrum of $(Ba_{1.97}Ce_{0.02})Ca_2B_4O_{10}$ recorded at room temperature. The emission spectrum was deconvoluted into four distinct Gaussian components from Ce^{3+} occupying the two inequivalent Ba^{2+} crystallographic sites. The inset presents a digital photograph of investigated phosphor under a 365 nm mercury lamp. (b) Room-temperature PLQY of $(Ba_{2-(3/2)x}Ce_x)Ca_2B_4O_{10}$ recorded under 355 nm excitation wavelength.

Substituting Ba^{2+} for Ce^{3+} within the $Ba_2Ca_2B_4O_{10}$ crystal structure leads to bright blue photoluminescence. Figure 2a presents the excitation and emission spectra of $(Ba_{1.97}Ce_{0.02})Ca_2B_4O_{10}$. The excitation spectrum (monitored at λ_{em} = 440 nm) spans from 280 to 400 nm and contains three distinct excitation bands centered at ≈285, ≈333, and ≈355 nm. These peaks stem from the absorption of the Ce^{3+} $4f^1$ ground-state electron ($^2F_{5/2}$) to a combination of different crystallographically independent substitution sites and the different energy levels within the 5d excited-state manifold. Exciting the phosphor with 355 nm radiation produced an intense, broad emission band with a total fwhm of 121 nm (≈6191 cm^{-1}). The emission spectrum can be described by four Gaussian peaks centered at 24,277 cm^{-1} (411 nm), 22,696 cm^{-1} (440 nm), 21,183 cm^{-1} (472 nm), and 19,017 cm^{-1} (525 nm). Each Ce^{3+} ion generates a spin−orbit-coupled $5d_1 \rightarrow {}^2F_{5/2}$, $^2F_{7/2}$ transition separated by ≈2000 cm^{-1}. The four peaks here, therefore, indicate the presence of two crystallographically independent Ce^{3+} emission centers. This was further confirmed through measurements of luminescence decay at room temperature, as illustrated in Figure S3. The curve can be described using a double exponential function, suggesting the presence of two distinct luminescence centers within the phosphor. The decay times for these centers were determined to be 16.28(5) and 35.96(1) ns, respectively. As also suggested indirectly by the structural refinements, Ce^{3+} appears only to occupy the two nonequivalent Ba^{2+} crystallographic sites, $[Ba(1)O_9]$ and $[Ba(2)O_7]$, resulting in the observed broad emission band. The refined average Ba−O bond length for the 9-fold coordinated barium is longer (2.93(1) Å) than for the 7-fold coordinated barium (2.79(3) Å). Consequently, the metal−ligand interactions are expected to be comparatively weaker at the 9-fold coordinated crystal site. This lower covalency results in weaker crystal field splitting, causing the Ce^{3+} substituted upon the $[Ba(1)O_9]$ position to produce a blue-shifted emission relative to Ce^{3+} on the $[Ba(2)O_7]$ site. This analysis was further supported by the empirical equation proposed by Van Uitert.[45] The energy of 5d → 4f luminescence in each distinct site can be estimated using eq 3

$$E = Q\left[1 - \left(\frac{V}{4}\right)^{1/V} 10^{-nE_a r/80}\right] \quad (3)$$

where Q stands for the d-band-edge position of the Ce^{3+}-free ion (50,000 cm^{-1}), V stands for the valence of Ce^{3+}, n represents the number of anions on the immediate shell around Ce^{3+}, and r is the radius of the host cation replaced by Ce^{3+}. According to the equation, the centers of the emission peaks are estimated to be 24,390 cm^{-1} (410 nm) and 19,762 cm^{-1} (506 nm) for Ce^{3+} substituted on $[Ba(1)O_9]$ and $[Ba(2)O_7]$, respectively. This shows excellent agreement with the data derived from the Gaussian deconvolution, indicating luminescence peaks centered at 411 and 472 nm. For comparison, calculating the peak positions for a hypothetical substitution of Ce^{3+} on the two Ca^{2+} crystallographic sites would yield red-shifted emission peaks centered at 17,857 cm^{-1} (560 nm) and 17,513 cm^{-1} (571 nm). Therefore, the optical spectroscopy corroborates the structural character-

https://doi.org/10.1021/acs.chemmater.3c01465
Chem. Mater. 2023, 35, 6491−6501

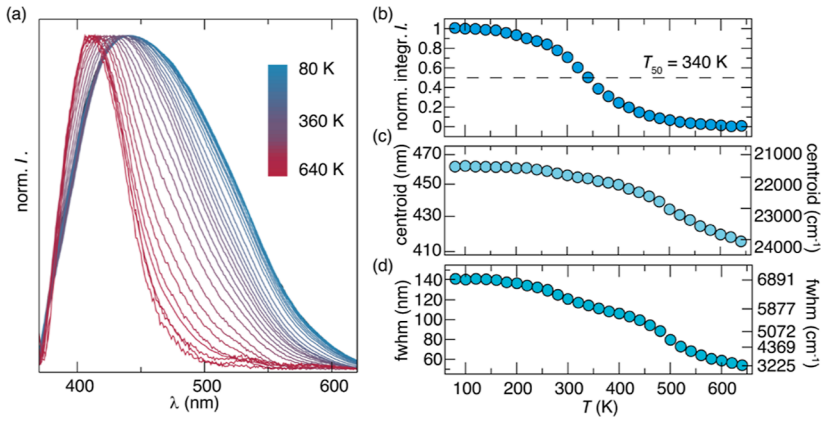

Figure 3. (a) Normalized luminescence spectra of the $(Ba_{1.97}Ce_{0.02})Ca_2B_4O_{10}$ phosphor recorded under λ_{ex} = 355 nm from 80 to 600 K. (b) Integrated intensity, (c) emission peak centroid, and (d) fwhm as a function of the temperature.

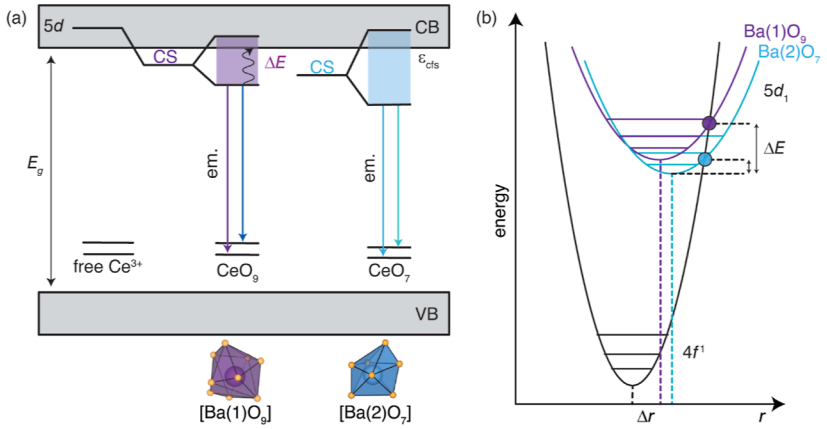

Figure 4. Schematic diagrams depicting thermal quenching of luminescence through (a) thermally activated photoionization where VB stands for the valence band, CS for the centroid shift, and CB for the conduction band and (b) thermally activated crossover process.

ization, which substantiates that Ce^{3+} exclusively occupies the Ba^{2+} positions.

The presence of Ce^{3+} luminescence originating from two distinct crystallographic sites was further validated by investigating the excitation and emission spectra evolution as a function of the monitoring wavelength. Measuring the excitation spectrum from λ_{em} = 430 to 530 nm in 20 nm increments (Figure S4a) shows that the higher energy peaks (≈290 and 325 nm) decrease in intensity with respect to the most intense excitation peak centered at ≈355 nm. On the other hand, recording the emission spectrum (Figure S4b) under various excitation wavelengths (315−355 nm) shows a slight red shift ($\lambda_{em,max}$ = 454 nm to $\lambda_{em,max}$ = 456 nm) and an increase in the fwhm from 131 nm (6467 cm^{-1}) to 147 nm (6860 cm^{-1}). It is clear that shorter excitation wavelengths preferentially excite the Ce^{3+} occupying the $[Ba(1)O_9]$ site with some minor contribution of Ce^{3+} on $[Ba(2)O_7]$. Conversely, longer wavelengths are required to sufficiently excite the Ce^{3+} on $[Ba(2)O_7]$. Analysis of the optical properties with different concentrations of Ce^{3+} provides additional information about this phosphor (Figure S5). Increasing the luminescent ion concentration in $Ba_2Ca_2B_4O_{10}$:Ce^{3+} causes the excitation and emission peaks to broaden. The origin of this trend can be explained by reabsorption related to the overlapping of the excitation and emission spectra on the high-energy side of the emission band. Furthermore, taking into account that Ce^{3+} ions occupy two crystallographically independent Ba^{2+} positions, the non-radiative energy transfer between Ce^{3+} ions can also cause a broadening of the emission band as a consequence of the energy transfer to the Ce^{3+} with the lower $5d_1$ state, which is going to be more efficient for higher Ce^{3+} concentrations. Additionally, also an inhomogeneous broadening of the luminescence bands from a random disorder around the active centers and an increase in the crystal field splitting strength can affect the broadening of the luminescence band as the concentration increases.

The luminescent efficiency for the complete series of the phosphors was determined by measuring the PLQY at room temperature with the results plotted in Figure 2b. At first, the PLQY increases along with increasing concentration of Ce^{3+} in the host structure. This is related to improved absorption of the incident excitation energy by the phosphor. The highest PLQY of 74(1)% was determined for $(Ba_{1.97}Ce_{0.02})Ca_2B_4O_{10}$. This value of PLQY nicely correlates with the calculated $\Theta_{D,DFT}$ = 532 K for the $Ba_2Ca_2B_4O_{10}$ host structure. Incorporating additional Ce^{3+} subsequently decreases the PLQY.[46] The origin of this process is likely due to concentration quenching arising from energy migration between neighboring Ce^{3+} ions.

3.2. Unanticipated Temperature-Dependent Response. Evaluating the practical application of phosphors for any lighting device requires additional investigations of the material's optical properties as a function of temperature. The

https://doi.org/10.1021/acs.chemmater.3c01465
Chem. Mater. 2023, 35, 6491−6501

normalized temperature-dependent luminescence spectra of $(Ba_{1.97}Ce_{0.02})Ca_2B_4O_{10}$ are plotted from 80 to 640 K using λ_{ex} = 355 nm in Figure 3a, and the raw data are provided in Figure S6. Calculating the normalized integrated intensity (norm. integr. I) shows that the emission remains nearly constant from 80 to 180 K. Further increasing the temperature decreases emission intensity due to the onset of thermal quenching. The calculated T_{50} is 340 K, as shown in Figure 3b. Regrettably, this is below the U.S. Department of Energy's expectations for a phosphor (T_{50} > 423 K). The temperature-dependent emission spectra also reveal a drastic blue shift in the centroid of the emission peak from ≈460 nm at 80 K to ≈415 nm at 640 K (Figure 3c). Even more surprising, the phosphor's fwhm is halved from 140 nm (≈6900 cm^{-1}) to only 58 nm (≈3200 cm^{-1}) across the same temperature range (Figure 3d).

The observed quenching of the 5d → 4f luminescence can be principally attributed to one of the two main mechanisms: thermally activated photoionization and thermally activated crossover quenching. Figure 4a depicts a simplified thermally activated photoionization process. The position of the ground-state 4f Ce^{3+} levels is unaffected by the Ce^{3+} substitution site because the 4f orbitals are strongly shielded from the influence of the surrounding ligands by the outer $5s^25p^6$ orbitals.[47] This prevents an overlap with the host's orbitals and minimizes their participation in chemical bonding. As a result, the effect of the centroid shift and crystal field splitting of the 4f orbitals may be neglected. On the contrary, the position of the 5d orbitals is highly dependent on variations in the coordination environment and the covalent nature of the metal−ligand bonds. Crystal field theory states that smaller coordination numbers, a decrease in the rare-earth−ligand bond length, and smaller polyhedral volumes should increase the magnitude of crystal field splitting, ultimately leading to a stabilization (decrease) in the excited $5d_1$ energy level.[48] The distance between the $5d_1$ level and the bottom of the conduction band (ΔE) influences the likelihood of thermally activated photoionization occurring. Exposing the phosphor to high temperatures causes the excited-state 5d electron wavefunction to couple with the conduction band (CB) wavefunctions efficiently. This coupling allows an electron to be more easily promoted from the excited $5d_1$ level to the conduction band, which results in a reduction or even complete quenching of light output. Considering the value of the bandgap of $Ba_2Ca_2B_4O_{10}$ is estimated to be 6.21 eV using a hybrid functional, the likelihood of quenching through photoionization is reduced. Additionally, the excited $5d_1$ level of the Ce^{3+} on the $[Ba(1)O_9]$ site should be closer to the conduction band's edge than Ce^{3+} on the $[Ba(2)O_7]$ site. Considering the spatial separation between $5d_1$ energy level(s) and the edge of the conduction band and the energy that would be necessary to overcome such a separation, luminescence quenching should occur first for $[Ce(1)O_9]$ rather than $[Ce(2)O_7]$. This would result in a red shift of the luminescence since the violet emission from Ce^{3+} on the 9-fold site would quench first, which contradicts what is experimentally observed. This indicates that a different mechanism is responsible for temperature quenching.

A more plausible mechanism for the observed quenching is thermally induced crossover that occurs when the ground- and excited-state potential energy surfaces intersect, as illustrated in Figure 4b. Absorption of radiation causes an electron to be excited from its 4f ground state to the 5d excited state. Excitation is also accompanied by a shift of the excited-state potential energy surface, Δr. Ideally, the excited-state electron relaxes down to the ground state through the emission of a photon. However, when the excited-state 5d potential energy surface is significantly displaced from the 4f ground state, the potential energy surfaces can intersect. This intersection, known as the crossover point, permits the energy of the $5d_1$ vibronic state to couple with the host's phonons, inducing non-radiative relaxation assisted by thermal energy to the ground 4f state. Thermally robust systems with respect to this quenching mechanism should have a small Δr. The magnitude of Δr can be approximated and analyzed by investigating the Stokes shift, which approximates parabolas offset between the ground and excited states. This is highly dependent on the Huang−Rhys parameter, which is associated with the magnitude of electron−phonon coupling. Based on the results of the Gaussian deconvolution of the emission spectra, the value of the Stokes shift is ≈ 6380 and ≈8561 cm^{-1} for the 9- and 7-fold coordinated Ce^{3+}, respectively. Consequently, the potential energy surface associated with Ce^{3+} on the $[Ba(2)O_7]$ site has a larger magnitude of electron−phonon coupling and thus should have a larger Δr than Ce^{3+} on $[Ba(1)O_9]$. This means that a crossover point is more likely to occur between the ground-state and excited-state potential energy surfaces of Ce^{3+} on the $[Ba(1)O_7]$ position.

$$I(T) = \frac{I_0}{1 + A_e^{(-\Delta E_a/k_B T)}} \tag{4}$$

In this case, the quenching mechanism can be described by the single-barrier model[49] (eq 4), where ΔE is the energy difference between the lowest vibrational level of the excited $5d_1$ state and the crossing point of the parabola, I_0 stands for the luminescence intensity in the limit of $T \to 0$ K, A is a fitting constant, and k_B is the Boltzmann constant. As derived from eq 4, when $\Delta E \ll k_B T$, the probability of thermal quenching via a crossover point is highly plausible. Scrutinizing the configuration coordinate diagram presented in Figure 4b suggests that with the increase of the temperature, the quenching process is expected to primarily transpire from Ce^{3+} in the 7-folded Ba^{2+} site because the activation energy responsible for non-radiative relaxation would be smaller compared to that of Ce^{3+} in the 9-folded Ba^{2+}. This agrees with the observations from the temperature-dependent luminescence spectroscopy that the lower energy emission peak quenches first. To support this hypothesis, we performed Gaussian deconvolution of temperature-dependent luminescence spectra in the 80−640 K range. As plotted in Figure S7a, the luminescence signal from the $Ce(1)O_7$ site has a faster quenching rate than from the $Ce(1)O_9$ site. Finally, above 540 K, only luminescence from the $Ce(1)O_9$ site can be observed and effectively deconvoluted by two Gaussian peaks, resulting from luminescence from the excited $5d_1$ level to the ^2F_J (J = 7/2, 5/2) states (Figure S7b). This indicates that the luminescence from the Ce^{3+} located in the seven-fold Ba^{2+} position is entirely quenched at high temperatures. The outcome of this site-selective quenching is a significant decrease in the fwhm of the emission peak (Figure 3d).

Site-selective quenching is a curious phenomenon that is occasionally observed in phosphors.[19,50,51] Not only does it affect the luminescence efficiency but it can also significantly impact the phosphor's observed emission color, as observed here. A closer examination of the optical properties in $(Ba_{1.97}Ce_{0.02})Ca_2B_4O_{10}$ shows a significant temperature-induced blue shift of the emission spectra, further impacting

https://doi.org/10.1021/acs.chemmater.3c01465
Chem. Mater. 2023, 35, 6491−6501

the phosphor's emission color. It is well known that increasing the temperature causes the crystal structure to expand, leading to longer rare-earth−ligand distances.[20] The result is a decrease in the covalency and magnitude of crystal field splitting around the Ce^{3+} ions, which causes the observed blue shift. The optimal approach for analyzing temperature-driven structural changes is with temperature-dependent powder X-ray diffraction. Figure S8a presents temperature-dependent powder X-ray diffractograms collected from 298 to 698 K for the $Ba_2Ca_2B_4O_{10}$ host structure. Following Le Bail refinements, it is clear that the crystal structure of the title phosphor is thermally stable with respect to decomposition or phase change across the temperature range studied. A shift of the diffraction peaks toward smaller angles occurs with increasing temperature, and the calculated volume of the unit cell increases from 981(1) to 1003(1) $Å^3$, as expected (Figure S8b). The magnitude of thermal expansion can be quantified by calculating the thermal expansion coefficient. The volumetric thermal expansion coefficient (α_V) can be determined using eq 5, where V corresponds to the volume of the unit cell, T indicates the temperature, and p stands for ambient pressure conditions. The calculated volumetric thermal expansion of $Ba_2Ca_2B_4O_{10}$ reaches $\alpha_V \approx 5.39 \times 10^{-5}$ K^{-1}.

$$\alpha_V = \frac{1}{V}\left(\frac{\partial V}{\partial T}\right)_p \tag{5}$$

To understand the magnitude of thermal expansion of $Ba_2Ca_2B_4O_{10}$, two other Ce^{3+}-substituted borate phosphors, $Ba_2Y_5B_5O_{17}$:Ce^{3+} and $Ba_3Y_2B_6O_{15}$:Ce^{3+}, were synthesized and analyzed by temperature-dependent powder X-ray diffraction from 298 to 658 K. The unit cell volumes of the synthesized samples were obtained by the Le Bail method, as plotted in Figure S9a,b. In each case, linear thermal expansion was observed. The resulting α_V values for these phosphors are provided in Table 2.

Table 2. Thermal Expansion Coefficients for Various Ce^{3+}- and Eu^{2+}-Substituted Phosphors

composition	thermal expansion coefficient, α_V (K^{-1})	refs
$Ba_2Ca_2B_4O_{10}$	5.39×10^{-5}	this work
$Ba_2Y_5B_5O_{17}$	3.90×10^{-5}	32
$Ba_3Y_2B_6O_{15}$	2.37×10^{-5}	25
$KSr(BH_4)_{2.80}Cl_{0.20}$	14.5×10^{-5}	52
$RbSr(BH_4)_{2.86}Cl_{0.14}$	9.2×10^{-5}	52
$CsSr(BH_4)_{2.74}Cl_{0.26}$	6.9×10^{-5}	52

The thermal expansion coefficient of $Ba_2Ca_2B_4O_{10}$ is nearly double than that of $Ba_2Y_5B_5O_{17}$ and $Ba_3Y_2B_6O_{15}$. Thus, a more dramatic change in the title phosphor's optical properties is expected compared to the other borate systems. Indeed, analyzing the temperature-dependent luminescence properties of $Ba_2Y_5B_5O_{17}$:Ce^{3+} shows that the compound undergoes a minor blue shift (476−467 nm) and a decrease in the emission fwhm from 114 nm (5489 cm^{-1}) to 107 nm (5155 cm^{-1}) at elevated temperatures (Figure 5a). Considering that this host has four crystallographically distinct sites for Ce^{3+} to occupy, the change in optical properties is most likely due to site-selective quenching. One of the best methods to evaluate chromaticity differences in emission spectra is by using the 1976 CIE $L^*u^*v^*$ (CIELUV) color space. Unlike the 1931 CIE XYZ color space, the CIE 1976 color space is designed to be perceptually uniform, meaning that numerical changes in the 1976 CIELUV coordinates correspond to a similar change in the perceived color difference.[53] Consequently, the phosphor's emission color was plotted on 1976 CIELUV color space, as shown in Figure 5b. Increasing the temperature causes the emission to shift, and the temperature-dependent chromaticity coordinates fall outside a three-step MacAdam ellipse. This implies that the emission stemming from $Ba_2Y_5B_5O_{17}$:Ce^{3+}, as can be seen by the average human eye, should have only a change in the perceived color at high temperatures. In comparison, the $\lambda_{em,max}$ of $Ba_3Y_2B_6O_{15}$:Ce^{3+} blue-shifts (464 to 457 nm) slightly as the temperature increases. This results in a slight change of color at elevated temperatures, as depicted in Figure S10a. The results agree with calculated thermal expansion coefficients for specific phosphors, as depicted in Table 2. $Ba_3Y_2B_6O_{15}$ experiences a smaller unit cell expansion than $Ba_2Y_5B_5O_{17}$, which results in a less significant blue shift of the emission peak as the temperature increases.

Examining the literature for a phosphor system that shows a more dramatic change in the emission peak brought to light the $ASr(BH_4)_{3-x}Cl_x$:Eu^{2+} (A = K, Rb, and Cs) system.[52] Figure 5c shows the normalized temperature-dependent luminescence spectra of $KSr(BH_4)_{2.80}Cl_{0.20}$:$Eu^{2+}$ from 110 to 475 K. A substantial blue shift of the emission peak occurs from $\lambda_{em,max}$ = 504 to 462 nm. Considering the structure that contains only one crystallographically independent Eu^{2+} substitution site, the change in the emission peak position cannot stem site-selective quenching. Plotting the emission color on a 1976 CIELUV diagram (Figure 5d) depicts the significant change in emission color moving from a saturated green to cyan. Analyzing the temperature-dependent powder X-ray diffractograms reveal that α_V is substantial (14.5×10^{-5} K^{-1}). Interestingly, the value of the thermal expansion coefficient decreases from A = K to A = Cs in $ASr(BH_4)_{3-x}Cl_x$:Eu^{2+} (A = K, Rb, and Cs). This directly affects the magnitude of the observed temperature-dependent blue shift from A = K to A = Cs, as shown in Figure S10b,c. The smaller K^+ atoms within the secondary coordination sphere of $[Sr(BH_4)_6]^{4-}$ can also get closer to the Eu^{2+} ions than the larger Rb^+ and Cs^+ ions, causing the Eu−B bonds to be longer when A = K^+, which can also contribute to the observed blue shift.

The combination of site-selective quenching and the impressive thermal expansion of $(Ba_{1.97}Ce_{0.02})Ca_2B_4O_{10}$ leads to two significant effects—a colossal blue shift of the emission peak and a substantial reduction of its fwhm, highlighted in Figure 5e. This observed optical response is the direct result of two simultaneous phenomena: thermally activated crossover and the thermal expansion of the unit cell. As temperature increases, the magnitude of electron−phonon coupling increases, causing the emission from Ce^{3+} on the $[Ba(2)O_7]$ site to quench first. This is directly reflected in the decreasing fwhm as a function of temperature and the substantial blue shift of the emission maximum. There is also a simultaneous increase in the volume of the unit cell and metal−ligand bond length (as expected due to the large thermal expansion coefficient of $Ba_2Ca_2B_4O_{10}$) with increasing the temperature leading to a decrease in the crystal field splitting, which further intensifies the magnitude of the blue shift. This leads to the perceptible change of luminescence color from cyan all the way to saturated violet, as plotted in Figure 5f.

https://doi.org/10.1021/acs.chemmater.3c01465
Chem. Mater. 2023, 35, 6491−6501

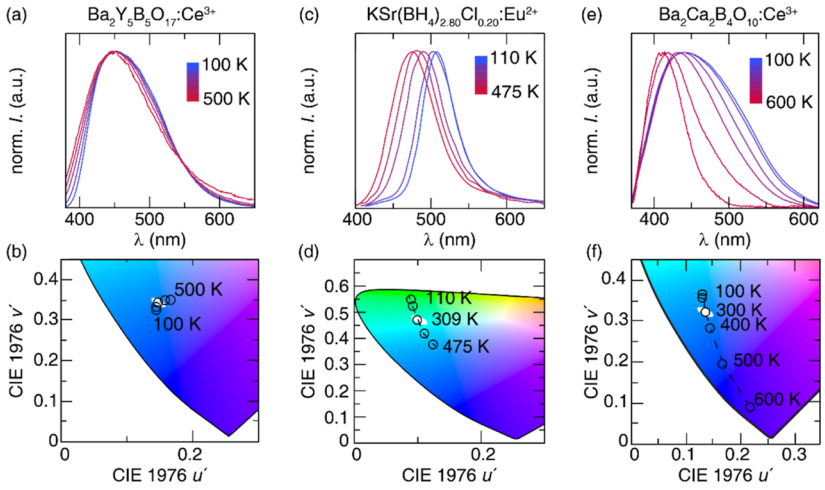

Figure 5. (a) Temperature-dependent luminescence spectra and (b) 1976 CIELUV chromaticity coordinates of $Ba_2Y_5B_5O_{17}:Ce^{3+}$ recorded under λ_{ex} = 380 nm from 100 to 500 K. (c) Temperature-dependent emission spectra of $KSr(BH_4)_{2.80}Cl_{0.20}:Eu^{2+}$ from 110 to 475 K under λ_{ex} = 330 nm. (d) 1976 CIELUV coordinates of $KSr(BH_4)_{2.80}Cl_{0.20}:Eu^{2+}$ calculated based on luminescence spectra in the 110−475 K range. (e) Luminescence spectra of $(Ba_{1.97}Ce_{0.02})Ca_2B_4O_{10}$ phosphor in the 100−600 K range under 355 nm excitation. (f) CIELUV coordinates of $(Ba_{1.97}Ce_{0.02})Ca_2B_4O_{10}$ phosphor.

3.3. Consequences of Chromatic Instability. For real-world LED light bulbs that operate at ≈423 K, it is imperative for phosphors to be thermally stable and withstand these temperatures. Thus, the phosphor used in commercial pc-LEDs should retain their optical properties, such as fwhm or $\lambda_{em,max}$, to ensure a consistent color output regardless of operating temperature. To demonstrate the impact of perceptible color change, a prototype white LED bulb was fabricated using a UV LED chip (λ_{ex} = 365 nm) coated with a phosphor blend of the chromatically unstable $(Ba_{1.97}Ce_{0.02})$-$Ca_2B_4O_{10}$ and two commercial phosphors: green-emitting β-SiAlON:Eu^{2+} and red-emitting $Sr_2Si_5N_8:Eu^{2+}$. The device produced cool white daylight at ambient conditions with a correlated color temperature (CCT) of 5562 K and a R_a = 93, as presented in Figure 6a. This R_a value surpasses LED daylight bulbs composed of InGaN, $Y_3Al_5O_{12}:Ce^{3+}$, and $Sr_2Si_5N_8:Eu^{2+}$, which typically have an $R_a \approx 80$.[53] The differences in the CRI R_a values can largely be attributed to the choice of LED. InGaN LEDs emit predominately monochromatic radiation at λ_{em} = 450 nm, causing a significant portion of the blue and violet region in the electromagnetic spectrum to be overlooked due to the narrow fwhm (<10 nm). This directly results in a low R_a. Using the UV LED and trichromatic phosphor blend allows the violet, blue, and cyan regions of the visible spectrum to be covered entirely, enhancing the color rendering and improving the visual experience.

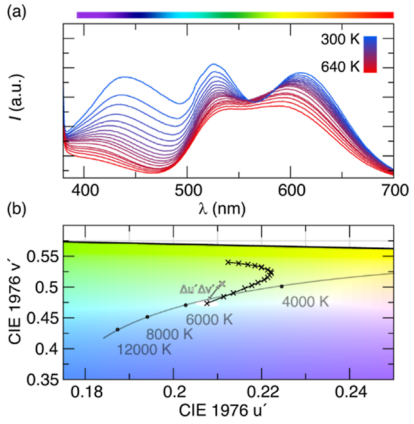

Figure 6. (a) Temperature-dependent emission spectra of a phosphor blend containing $Ba_2Ca_2B_4O_{10}:Ce^{3+}$, β-SiAlON:Eu^{2+}, and $Sr_2Si_5N_8:Eu^{2+}$ recorded under λ_{ex} = 365 nm measured from 300 to 640 K. (b) White light device's output color is plotted on 1976 CIELUV color coordinate as a function of temperature from 300 to 640 K. The gray line indicates the position of the Planckian locus. The white ellipse represents a three-step MacAdam ellipse.

The prototype device clearly generates a high-color-quality white light due to nearly complete coverage of the visible spectrum. However, it should be noted that this white light spectrum was collected at room temperature. The poor chromatic stability of $(Ba_{1.97}Ce_{0.02})Ca_2B_4O_{10}$ is likely to impact the quality of the white light as the operating temperature of the prototype increases. Temperature-dependent emission spectra of the prototype were thus collected and are provided in Figure 6a. Unsurprisingly, there is a notable change in the blue region of the white light spectrum. Not only does the emission from $(Ba_{1.97}Ce_{0.02})Ca_2B_4O_{10}$ decreases in intensity due to thermal quenching but the colossal blue shift is also observed. Interestingly, the commercial phosphors also exhibit chromatic instabilities: β-SiAlON:Eu^{2+} slightly red-shifts, whereas $Sr_2Si_5N_8:Eu^{2+}$ blue-shifts. All of the phosphors show a decrease in the emission intensity, with the borate losing nearly all emission intensity by 640 K.

Analyzing the color change of the white light spectrum as a function of temperature on the 1976 CIELUV diagram (Figure 6b) shows that the light's color point moves dramatically from a cold white to green. This shift in color can be quantified by determining the distance from the initial room-temperature color coordinates, $(u_{init.}', v_{init.}')$, to the average color coordinate measured as a function of temperature $(u_{avg.}', v_{avg.}')$. The resulting $\Delta u'\Delta v'$ can then be calculated following the distance formula expressed by eq 6.

$$\Delta u'\Delta v' = \sqrt{(u'_{avg.} - u'_{init.})^2 + (v'_{avg.} - v'_{init.})^2} \quad (6)$$

As shown here, there is a significant shift in the color of the device where $\Delta u'\Delta v' = 0.0244(6)$ going from room temper-

https://doi.org/10.1021/acs.chemmater.3c01465
Chem. Mater. 2023, 35, 6491−6501

ature to 640 K. Plotting a three-step MacAdam ellipse centered at room-temperature (300 K) chromaticity coordinates shows that by increasing the temperature by just 20−320 K creates a perceptible shift in the observed color. When the temperature reaches 420 K, the device's output color has moved from cold-white to yellow-green, making the device unusable as an energy-efficient white light as the perceived color is entirely different from the starting white at room temperature.

4. CONCLUSIONS

A Ce^{3+}-substituted $Ba_2Ca_2B_4O_{10}$ phosphor was successfully synthesized using a high-temperature solid-state synthesis. Synchrotron powder X-ray diffraction confirmed the phase purity of the obtained products and suggested that Ce^{3+} exclusively substituted on the two crystallographically independent Ba^{2+} sites. Exciting this phosphor with UV radiation (λ_{ex} = 355 nm) produced a broadband blue emission arising from the dual-site occupancy of Ce^{3+} on the two independent Ba^{2+} sites. The compound generated an impressive PLQY of 74(1)% at room temperature. Unfortunately, temperature-dependent luminescence measurements revealed a remarkable thermally induced blue shift from ≈460 to 410 nm and a significant reduction of the fwhm. The unusual behavior was determined to stem from two phenomena. First, as the temperature increases, the Ce^{3+} occupying the [BaO_7] site preferentially quenches, causing the emission fwhm to decrease drastically. This phenomenon is accompanied by a large thermal expansion, which leads to an elongation of the activator−ligand bond lengths that induces a blue shift of the emission spectra. Temperature-dependent X-ray diffraction showed that the phosphor has a significant thermal expansion coefficient of $\alpha_V = 5.4 \times 10^{-5}$ K^{-1}, nearly double that of related borate phosphors. Combining these two mechanisms leads to an unprecedented change in the phosphor's chromatic coordinates. The effect of chromatic instabilities on pc-LEDs was highlighted by fabricating a prototype using a UV LED and a phosphor blend composed of commercially available green- and red-emitting phosphors with blue-emitting $Ba_2Ca_2B_4O_{10}$:Ce^{3+}. Operating this device at high temperatures unveiled a drastic change in the emission color from white to yellow-green due to the gradual loss of the blue component. This significantly impacts the perceived color by the average human eye. These findings offer valuable insights into the potential causes of chromatic instabilities in luminescent materials, which can affect the observed emission color while demonstrating the dramatic impact of chromatic shifts on energy-efficient white LED lighting.

■ ASSOCIATED CONTENT

Supporting Information

The Supporting Information is available free of charge at https://pubs.acs.org/doi/10.1021/acs.chemmater.3c01465.

Powder X-ray diffractograms, Rietveld refinements, luminescence decays, emission spectra excited at different wavelengths and concentrations of Ce^{3+}, temperature-dependent emission spectra and its analysis, temperature-dependent X-ray diffraction patterns, CIE-LUV coordinates, and refined atomic coordinates and isotropic displacement parameters (PDF)

■ AUTHOR INFORMATION

Corresponding Author

Jakoah Brgoch − *Department of Chemistry, University of Houston, Houston, Texas 77204, United States; Texas Center for Superconductivity, University of Houston, Houston, Texas 77204, United States;* orcid.org/0000-0002-1406-1352; Email: jbrgoch@uh.edu

Authors

Małgorzata Sójka − *Department of Chemistry, University of Houston, Houston, Texas 77204, United States; Texas Center for Superconductivity, University of Houston, Houston, Texas 77204, United States;* orcid.org/0000-0001-9346-8929

Shruti Hariyani − *Department of Chemistry, University of Houston, Houston, Texas 77204, United States; Texas Center for Superconductivity, University of Houston, Houston, Texas 77204, United States;* orcid.org/0000-0002-4707-8863

Nakyung Lee − *Department of Chemistry, University of Houston, Houston, Texas 77204, United States; Texas Center for Superconductivity, University of Houston, Houston, Texas 77204, United States*

Complete contact information is available at: https://pubs.acs.org/10.1021/acs.chemmater.3c01465

Notes

The authors declare no competing financial interest.

■ ACKNOWLEDGMENTS

The authors thank the National Science Foundation (DMR-1847701) for funding this research. This work used the resources available through the 11-BM beamline at the Advanced Photon Source, an Office of Science User Facility operated for the U.S. Department of Energy (DOE) Office of Science by Argonne National Laboratory, under Contract no. DE-AC02- 06CH11357. This work used the Opuntia/Sabine/Carya cluster(s) operated by the Research Computing Data Core at the University of Houston.

■ REFERENCES

(1) George, N. C.; Denault, K. A.; Seshadri, R. Phosphors for Solid-State White Lighting. *Annu. Rev. Mater. Res.* **2013**, *43*, 481−501.

(2) Pust, P.; Schmidt, P. J.; Schnick, W. A Revolution in Lighting. *Nat. Mater.* **2015**, *14*, 454−458.

(3) Grand View Research. *LED Lighting Market Size, Share & Trends Analysis Report By Product (Lamps, Luminaires), By Application (Indoor, Outdoor), By End-Use (Commercial, Residential, Industrial), By Region, And Segment Forecasts, 2023−2030*: San Francisco, 2022.

(4) Bachmann, V.; Ronda, C.; Meijerink, A. Temperature Quenching of Yellow Ce^{3+} Luminescence in YAG:Ce. *Chem. Mater.* **2009**, *21*, 2077−2084.

(5) Brinkley, S. E.; Pfaff, N.; Denault, K. A.; Zhang, Z.; Bert Hintzen, H. T.; Seshadri, R.; Nakamura, S.; DenBaars, S. P. Robust Thermal Performance of $Sr_2Si_5N_8$:Eu^{2+} : An Efficient Red Emitting Phosphor for Light Emitting Diode Based White Lighting. *Appl. Phys. Lett.* **2011**, *99*, 241106.

(6) Lin, Y.-C.; Karlsson, M.; Bettinelli, M. Inorganic Phosphor Materials for Lighting. *Top. Curr. Chem.* **2016**, *374*, 21.

(7) Mo, C.; Fang, W.; Pu, Y.; Liu, H.; Jiang, F. Growth and Characterization of InGaN Blue LED Structure on Si(111) by MOCVD. *J. Cryst. Growth* **2005**, *285*, 312−317.

(8) Zhuo, Y.; Mansouri Tehrani, A.; Oliynyk, A. O.; Duke, A. C.; Brgoch, J. Identifying an Efficient, Thermally Robust Inorganic Phosphor Host via Machine Learning. *Nat. Commun.* **2018**, *9*, 4377.
(9) Li, S.; Wang, L.; Tang, D.; Cho, Y.; Liu, X.; Zhou, X.; Lu, L.; Zhang, L.; Takeda, T.; Hirosaki, N.; Xie, R. J. Achieving High Quantum Efficiency Narrow-Band β-SiAlON:Eu^{2+} Phosphors for High-Brightness LCD Backlights by Reducing the Eu^{3+} Luminescence Killer. *Chem. Mater.* **2018**, *30*, 494−505.
(10) Sharma, S. K.; Lin, Y. C.; Carrasco, I.; Tingberg, T.; Bettinelli, M.; Karlsson, M. Weak Thermal Quenching of the Luminescence in the $Ca_3Sc_2Si_3O_{12}$:Ce^{3+} Garnet Phosphor. *J. Mater. Chem. C* **2018**, *6*, 8923−8933.
(11) Yang, L. X.; Xu, X.; Hao, L. Y.; Wang, Y. F.; Yin, L. J.; Yang, X. F.; He, W.; Li, Q. X. Optimization Mechanism of $CaSi_2O_2N_2$:Eu^{2+} Phosphor by La^{3+} Ion Doping. *J. Phys. D: Appl. Phys.* **2011**, *44*, 355403.
(12) Yoshimura, K.; Fukunaga, H.; Izumi, M.; Takahashi, K.; Xie, R.-J.; Hirosaki, N. Achieving superwide-color-gamut display by using narrow-band green-emitting γ-AlON:Mn,Mg phosphor. *Jpn. J. Appl. Phys.* **2017**, *56*, 041701.
(13) Cai, J.; Pan, H.; Wang, Y. Synthesis and Luminescence Properties of Ca_2SiO_4-Based Red Phosphors with Sm^{3+} Doping for White LEDs. *Int. J. Miner., Metall. Mater.* **2012**, *19*, 663−667.
(14) Piao, X.; Machida, K.; Horikawa, T.; Hanzawa, H.; Shimomura, Y.; Kijima, N. Preparation of $CaAlSiN_3$:Eu^{2+} Phosphors by the Self-Propagating High-Temperature Synthesis and Their Luminescent Properties. *Chem. Mater.* **2007**, *19*, 4592−4599.
(15) Zhang, C.; Uchikoshi, T.; Xie, R.-J.; Liu, L.; Cho, Y.; Sakka, Y.; Hirosaki, N.; Sekiguchi, T. Reduced Thermal Degradation of the Red-Emitting $Sr_2Si_5N_8$:Eu^{2+} Phosphor via Thermal Treatment in Nitrogen. *J. Mater. Chem. C* **2015**, *3*, 7642−7651.
(16) Pust, P.; Weiler, V.; Hecht, C.; Tücks, A.; Wochnik, A. S.; Henß, A. K.; Wiechert, D.; Scheu, C.; Schmidt, P. J.; Schnick, W. Narrow-Band Red-Emitting $Sr[LiAl_3N_4]$:Eu^{2+} as a next-Generation LED-Phosphor Material. *Nat. Mater.* **2014**, *13*, 891−896.
(17) Kim, K. B.; Kim, Y. I.; Chun, H. G.; Cho, T. Y.; Jung, J. S.; Kang, J. G. Structural and Optical Properties of $BaMgAl_{10}O_{17}$:Eu^{2+} Phosphor. *Chem. Mater.* **2002**, *14*, 5045−5052.
(18) Bizarri, G.; Moine, B. On Phosphor Degradation Mechanism: Thermal Treatment Effects. *J. Lumin.* **2005**, *113*, 199−213.
(19) Hariyani, S.; Xing, X.; Amachraa, M.; Bao, J.; Ong, S. P.; Brgoch, J. Realizing Wide-Gamut Human-Centric Display Lighting with $K_3AlP_3O_9N$:Eu^{2+}. *Adv. Opt. Mater.* **2023**, *11*, 2202689.
(20) Brites, C. D. S.; Balabhadra, S.; Carlos, L. D. Lanthanide-Based Thermometers: At the Cutting-Edge of Luminescence Thermometry. *Adv. Opt. Mater.* **2019**, *7*, 1801239.
(21) Zheng, T.; Sójka, M.; Runowski, M.; Woźny, P.; Lis, S.; Zych, E. Tm^{2+} Activated SrB_4O_7 Bifunctional Sensor of Temperature and Pressure—Highly Sensitive, Multi-Parameter Luminescence Thermometry and Manometry. *Adv. Opt. Mater.* **2021**, *9*, 2101507.
(22) https://www.usailighting.com/stuff/contentmgr/files/1/f386756b8bcf5da65a8d3c26a56b82e7/misc/macadam_faqs.pdf (accessed May 22, 2023).
(23) Zhong, J.; Zhuo, Y.; Hariyani, S.; Zhao, W.; Wen, J.; Brgoch, J. Closing the Cyan Gap Toward Full-Spectrum LED Lighting with $NaMgBO_3$:Ce^{3+}. *Chem. Mater.* **2020**, *32*, 882−888.
(24) Sun, X.; Zhang, C.; Wu, J.; Zhu, P.; Zhang, X.; Hang, Y. A Novel Blue-Emitting $KCa_4(BO_3)_3$:Ce^{3+} Phosphor for White LED Application. *J. Rare Earths* **2016**, *34*, 571−575.
(25) Duke, A. C.; Hariyani, S.; Brgoch, J. $Ba_3Y_2B_6O_{15}$:Ce^{3+} —A High Symmetry, Narrow-Emitting Blue Phosphor for Wide-Gamut White Lighting. *Chem. Mater.* **2018**, *30*, 2668−2675.
(26) Liebertz, J.; Fröhlich, R. Struktur Und Kristallchemie von Ba2M(B3O6)2 Mit M = Ca, Cd, Mg, Co Und Ni. *Z. Kristallogr. N. Cryst. Struct.* **1984**, *168*, 293−297.
(27) Akella, A.; Keszler, D. A. Crystal Structure of the Borate $Ba_2Ca(BO_3)_2$. *Main Group Met. Chem.* **1995**, *18*, 35−42.
(28) Liu, L.; Zhang, F.; Pan, S.; Lei, C.; Zhang, F.; Dong, X.; Wang, Z.; Yu, H.; Yang, Z. Synthesis, crystal structure and properties of a new barium calcium borate,$Ba_2Ca_2(B_2O_5)_2$. *Solid State Sci.* **2015**, *39*, 105−109.
(29) Xiao, F.; Xue, Y. N.; Ma, Y. Y.; Zhang, Q. Y. $Ba_2Ca(B_3O_6)_2$:Eu^{2+},Mn^{2+}: A Potential Tunable Blue-White-Red Phosphors for White Light-Emitting Diodes. *Phys. B* **2010**, *405*, 891−895.
(30) Lin, H.; Liang, H.; Tian, Z.; Han, B.; Wang, J.; Su, Q.; Zhang, G. Luminescence of $Ba_2Ca(BO_3)_2$:Ce^{3+} —Influence of Charge Compensator, Energy Transfer and LED Application. *J. Phys. D: Appl. Phys.* **2009**, *42*, 165409.
(31) Guo, C.; Luan, L.; Xu, Y.; Gao, F.; Liang, L. White Light−Generation Phosphor $Ba_2Ca(BO_3)$:Ce^{3+}, Mn^{2+} for Light-Emitting Diodes. *J. Electrochem. Soc.* **2008**, *155*, J310.
(32) Hermus, M.; Phan, P.-C.; Brgoch, J. Ab Initio Structure Determination and Photoluminescent Properties of an Efficient, Thermally Stable Blue Phosphor, $Ba_2Y_5B_5O_{17}$:Ce^{3+}. *Chem. Mater.* **2016**, *28*, 1121−1127.
(33) Toby, B. H. EXPGUI, a Graphical User Interface for GSAS. *J. Appl. Crystallogr.* **2001**, *34*, 210−213.
(34) Momma, K.; Izumi, F. VESTA 3 for Three-Dimensional Visualization of Crystal, Volumetric and Morphology Data. *J. Appl. Crystallogr.* **2011**, *44*, 1272−1276.
(35) de Mello, J. C.; Wittmann, F. H.; Friend, R. H. An Improved Experimental Determination of External Photoluminescence Quantum Efficiency. *Adv. Mater.* **1997**, *9*, 230−232.
(36) Kresse, G.; Furthmüller, J. Efficient Iterative Schemes for Ab Initio Total-Energy Calculations Using a Plane-Wave Basis Set. *Phys. Rev. B: Condens. Matter Mater. Phys.* **1996**, *54*, 11169−11186.
(37) Blöchl, P. E. Projector Augmented-Wave Method. *Phys. Rev. B: Condens. Matter Mater. Phys.* **1994**, *50*, 17953−17979.
(38) Perdew, J. P. Density Functional Theory and the Band Gap Problem. *Int. J. Quantum Chem.* **2009**, *28*, 497−523.
(39) Wu, Z.; Zhao, E.; Xiang, H.; Hao, X.; Liu, X.; Meng, J. Crystal Structures and Elastic Properties of Superhard IrN_2 and IrN_3 from First Principles. *Phys. Rev. B: Condens. Matter Mater. Phys.* **2007**, *76*, 054115.
(40) Heyd, J.; Scuseria, G. E.; Ernzerhof, M. Hybrid Functionals Based on a Screened Coulomb Potential. *J. Chem. Phys.* **2003**, *118*, 8207−8215.
(41) Wang, V.; Xu, N.; Liu, J. C.; Tang, G.; Geng, W. T. VASPKIT: A User-Friendly Interface Facilitating High-Throughput Computing and Analysis Using VASP Code. *Comput. Phys. Commun.* **2021**, *267*, 108033.
(42) Zhuo, Y.; Hariyani, S.; Zhong, J.; Brgoch, J. Creating a Green-Emitting Phosphor through Selective Rare-Earth Site Preference in $NaBaB_9O_{15}$:Eu^{2+}. *Chem. Mater.* **2021**, *33*, 3304−3311.
(43) Hafner, J. A. A note on Vegard's and Zen's laws. *J. Phys. F: Met. Phys.* **1985**, *15*, L43−L48.
(44) Shannon, R. D. Revised Effective Ionic Radii and Systematic Studies of Interatomic Distances in Halides and Chalcogenides. *Acta Crystallogr., Sect. A: Found. Adv.* **1976**, *32*, 751−767.
(45) Van Uitert, L. G. An Empirical Relation Fitting the Position in Energy of the Lower d-Band Edge for Eu^{2+} or Ce^{3+} in Various Compounds. *J. Lumin.* **1984**, *29*, 1−9.
(46) Tanner, P. A.; Zhou, L.; Duan, C.; Wong, K.-L. Misconceptions in Electronic Energy Transfer: Bridging the Gap between Chemistry and Physics. *Chem. Soc. Rev.* **2018**, *47*, 5234−5265.
(47) Dorenbos, P. Modeling the Chemical Shift of Lanthanide 4f Electron Binding Energies. *Phys. Rev. B: Condens. Matter Mater. Phys.* **2012**, *85*, 165107.
(48) Qin, X.; Liu, X.; Huang, W.; Bettinelli, M.; Liu, X. Lanthanide-Activated Phosphors Based on 4f-5d Optical Transitions: Theoretical and Experimental Aspects. *Chem. Rev.* **2017**, *117*, 4488−4527.
(49) Mott, N. F. On the Absorption of Light by Crystals. *Proc. R. Soc. London, Ser. A* **1938**, *167*, 384−391.
(50) Hariyani, S.; Brgoch, J. Advancing Human-Centric LED Lighting Using Na_2MgPO_4F:Eu^{2+}. *ACS Appl. Mater. Interfaces* **2021**, *13*, 16669−16676.
(51) Qiao, J.; Ning, L.; Molokeev, M. S.; Chuang, Y.-C.; Liu, Q.; Xia, Z. Eu^{2+} Site Preferences in the Mixed Cation $K_2BaCa(PO_4)_2$ and

https://doi.org/10.1021/acs.chemmater.3c01465
Chem. Mater. 2023, 35, 6491−6501

Thermally Stable Luminescence. *J. Am. Chem. Soc.* **2018**, *140*, 9730−9736.
(52) Wylezich, T.; Sontakke, A. D.; Castaing, V.; Suta, M.; Viana, B.; Meijerink, A.; Kunkel, N. One Ion, Many Facets: Efficient, Structurally and Thermally Sensitive Luminescence of Eu^{2+} in Binary and Ternary Strontium Borohydride Chlorides. *Chem. Mater.* **2019**, *31*, 8957−8968.
(53) Hariyani, S.; Brgoch, J. Spectral Design of Phosphor-Converted LED Lighting Guided by Color Theory. *Inorg. Chem.* **2022**, *61*, 4205−4218.

https://doi.org/10.1021/acs.chemmater.3c01465
Chem. Mater. 2023, 35, 6491−6501